Chemical Engineering Journal 156 (2010) 594–600

Contents lists available at ScienceDirect

Chemical Engineering Journal

journal homepage: www.elsevier.com/locate/cej

Semi-batch reactive crystallisation of mono-ammonium phosphate: An experimental study

Johan Utomo[a,*], Yusuke Asakuma[b], Nicoleta Maynard[a], Kouji Maeda[b], Keisuke Fukui[b], Moses O. Tadé[a]

[a] Department of Chemical Engineering, Curtin University of Technology, GPO Box U1987, Perth, Western Australia 6845, Australia
[b] Department of Mechanical and System Engineering, University of Hyogo, 2167 Shosha, Himeji City, Hyogo 671-2280, Japan

ARTICLE INFO

Article history:
Received 23 October 2008
Received in revised form 13 April 2009
Accepted 14 April 2009

Keywords:
Ammonium phosphate
Reactive crystallisation
Semi-batch crystalliser
Crystal size distribution

ABSTRACT

$NH_4H_2PO_4$, mono-ammonium phosphate (MAP) and $(NH_4)_2HPO_4$, di-ammonium phosphate (DAP) have become leading phosphate fertiliser products worldwide. Ammonium phosphates are produced by reactions of ammonia and phosphoric acid resulting in the formation of the mono-basic, di-basic, or tri-basic salts. Inefficiencies in the MAP/DAP production process are due to the lack of a fundamental understanding of the crystallisation–reaction mechanisms. A semi-batch reactive crystalliser equipped with a cooling jacket, a dual feed system and a turbine type agitator has been used in this study. Effects of N/P ratio, seed crystals, feeding system, feed flow rate, initial supersaturation, feeding time and mixing intensity to the real-time supersaturation, crystal yield, crystal shape (aspect ratio) and final crystal size distribution (CSD) were studied in order to understand the kinetics. This study aims to provide new insights into the MAP/DAP reaction–crystallisation mechanisms.

1. Introduction

Ammonium phosphates are produced by reactions (precipitation) between ammonia and phosphoric acid resulting in the formation of mono-basic, di-basic or tri-basic salts. When the mole ratio of nitrogen from ammonia and phosphorus from phosphoric acid is 1.0, mono-ammonium phosphate (MAP—$NH_4H_2PO_4$) is formed, and when the mole ratio is 2.0, di-ammonium phosphate (DAP—$(NH_4)_2HPO_4$) is formed. The reaction is exothermic, so the MAP and DAP are produced at an elevated and relatively constant temperature of 110 °C. The equations for the neutralization reaction between ammonia and phosphoric acid are as follows:

$$NH_3(g) + H_3PO_4(aq) \rightarrow NH_4H_2PO_4(s)$$

$$NH_3(g) + NH_4H_2PO_4(aq) \rightarrow (NH_4)_2HPO_4(s)$$

$$NH_3(g) + (NH_4)_2HPO_4(aq) \rightarrow (NH_4)_3PO_4(s)$$

The mono-ammonium phosphate (MAP) tends to produce needle forms of crystals while the di-ammonium phosphate (DAP) results in more granular forms of crystals. Tri-ammonium phosphate (TAP—$(NH_4)_3PO_4$) is an unstable crystal and less soluble than MAP and DAP. MAP and DAP are used as a main source of phosphorus in fertilisers. Several important characteristics of MAP, DAP and TAP are identified in Table 1 [1].

Work in reactive crystallisation research has not been as popular as non-reactive crystallisation work. Most reactive crystallisation work was conducted in liquid–liquid and some of them in gas–liquid. The applications range from calcium oxalate [2], benzoic acid [3,4], calcium carbonate [5,6], barium sulphate [7,8], barium carbonate [9,10], potassium dihydrogen phosphate [11], and many others. Kotaki and Tsuge [12] undertook a reactive crystallisation of calcium carbonate by gas–liquid reactions in a seeded and non-seeded batch crystalliser. They concluded that the crystal growth of an non-seeded system was controlled by primary nucleation and followed by secondary nucleation. Tavare and Garside [13] performed a simulation on liquid–liquid reactive crystallisation in a semi-batch crystalliser. They examined the effects of reaction kinetics, nucleation kinetics and a feed addition profile on product characteristics and compared these with the corresponding results for a batch crystalliser. They found that a reaction engineering approach can be used in the modelling procedure; such simulation could suggest a starting point for experimental studies, and the feed addition profile was the most significant factor in controlling the crystal size distribution. The importance of mixing in the reactive crystallisation process was captured by the recent work of Abbasi and Alamdari [14] who studied the mixing effects on CSD in the semi-batch reactive crystallisation of manganese ethylenebis. It was found that, for reactive crystallisation, both meso- and micro-mixing are the

* Corresponding author. Tel.: +61 8 9266 7610; fax: +61 8 9266 2681.
E-mail address: johan.utomo@gmail.com (J. Utomo).

1385-8947/$ – see front matter © 2009 Elsevier B.V. All rights reserved.
doi:10.1016/j.cej.2009.04.055

Nomenclature

Notation

c	solute concentration (g/g solution or g/100 g solution)
T	temperature (°C)
Δc	supersaturation degree in concentration (g/g solution or g/100 g solution)
ΔT	supersaturation degree in temperature (°C)
Q	flow rate of reactant (g/min)

most influential factors because the reactions take place on a molecular scale. The uniqueness of the nature of reactive crystallisation and the complexity of its model challenge us to explore the reactive crystallisation of mono-ammonium phosphate in a semi-batch crystalliser in order to understand the underlying mechanisms and interactions on the reactions and crystallisation processes.

The work of ammonium phosphates reactive crystallisation research is, however, limited only in the scope of impurities effect. The conventional process of producing ammonium phosphate from phosphoric acid was modified, as explained by the work of Zhong et al. [15]. They modified the ammonium phosphate production process which needed a high quality of ore (APPAC process) in the process, with a slurry concentration that can utilise middle and low quality of ore. A high impurity content that can cause a scaling and blocking problem in the acid concentrator heater may be avoided by applying the modified process. Recent work by Campbell et al. [16] in Australia reported the impact of impurities on the ammonium phosphates slurry characteristics, which cause several problems in mixing, flow ability and pumping efficiency. These factors contribute to the unit process/plant efficiency. They found that hydrolysis of metal ions (Fe^{3+} and Al^{3+}) initiate solids formation as they act as nucleation sites for crystallisation. In industry, the hydrolysis process leads to some challenges and causes inefficiencies. This is due to a high recycle ratio in the granulation process, the fluidity of the slurry, and uncontrolled product size distribution, which further triggers a domino effect that can decrease the downstream unit's efficiency and produce an off specification product. Although these commodities are commercially produced and matured in research, some challenges in the crystallisation kinetics, and solubility still remain and have not yet been addressed. The need of MAP crystallisation models in order to predict, design and optimise the process is critical.

In order to study them, the following approaches were taken. Firstly, MAP was produced from pure phosphoric acid by a single feed of ammonia solution. N/P molar ratio, initial concentration of phosphoric acid, effect of seeding policy and supersaturation were studied in order to obtain more insights into the reaction and crystallisation mechanisms. Several variables, such as pH, temperature, MAP concentration in solution, suspension density, and mean crystal size were gathered. Secondly, MAP was produced by a dual feed system of phosphoric acid and ammonia solution. A saturated or supersaturated MAP solution was used as a starting solution. The feed flow rate, feeding time, seeding effect, initial supersaturation, mixing effect, and initial concentration effects on product characteristics were studied thoroughly. The same output variables were observed in order to understand the effects of studied factors and to clarify the reaction and crystallisation mechanisms of the MAP system.

2. Experimental setup

As shown in Fig. 1, a half litre, closed-jacketed vessel equipped with a dual feed system and a turbine type agitator was used as a reactor and crystalliser. The reaction was conducted at 10–20 °C and 300 rpm. A 28 wt% ammonia solution and a phosphoric acid 40 wt% solution was used as reactant(s) and fed into a saturated MAP solution. A temperature controller, a pH controller, and a conductivity meter were used to manipulate, monitor and record the process variable evolution through the reaction time.

Firstly, a saturated mono-ammonium phosphate solution was made according to its saturation temperature. Once the temperature was ready, the dual feeding system was started. Cooling water temperature was set constant at 10 °C/15 °C/20 °C. The conductivity probe had a range from 2.0 S/m to 19.99 S/m. Temperature, pH and conductivity output data were transferred and recorded in a data logger. For the single feed system, a NH_3 solution was fed into and H_3PO_4 solution with different concentrations initially placed inside the crystalliser. For the seeded system, a certain amount of seed was placed at the same time as the first droplet of reactant(s) fed into to the crystalliser. In the phosphoric acid system, the N/P molar ratio and phosphoric acid concentration were the key variables to be investigated while, in the MAP system, the effects of reaction time, supersaturation and seed amount on the crystal size distribution were examined.

Lastly, the slurry was filtered, washed and dried. The crystal size distribution was measured by a laser diffraction apparatus (Microtrac®) and a sieving method. The number of crystal was calculated from the mass of dry crystals. The conductivity data was converted into the concentration of solute MAP in the solution by using the technique reported in Ref. [17].

3. Results and discussion

3.1. Single feed system

As can be seen in Table 2, N/P ratio results have significant effects on CSD. Mean size based on volume (MV) increases from 250 μm to 450 μm as N/P increases (up to N/P = 1) and then decreases to 360 μm. An inverse trend appeared in the mean size based on the number (MN). MN reduced from 110 μm to 15 μm. Smaller crystals are produced when the ratio increased. The N/P molar ratio produces a different degree of supersaturation (Δc) which governs the product size distribution. From the CSD profiles in Fig. 2, the low

Table 1
Properties of ammonium phosphates salts (MAP, DAP and TAP).

Properties	$NH_4H_2PO_4$ (mono-ammonium phosphate)	$(NH_4)_2HPO_4$ (di-ammonium phosphate)	$(NH_4)_3PO_4$ (tri-ammonium phosphate)
Molar mass (g/mol)	115	132	149
Specific gravity @ 20 °C	1.803	1.619	N/A
Heat of formation (cal)	29,000	48,500	58,400
Melting point (°C)	190	N/A	N/A
Solubility @ 25 °C (g/g water)	40	69.5	17.7
Ammonia vapor pressure @ 100 °C and 125 °C (mmHg)	0.00 and 0.05	5.00 and 30.0	643 and 1177
pH of 0.1 M solution	4.4	8.0	9.4
Crystal form	Tetragonal	Monoclinic	Orthorhombic

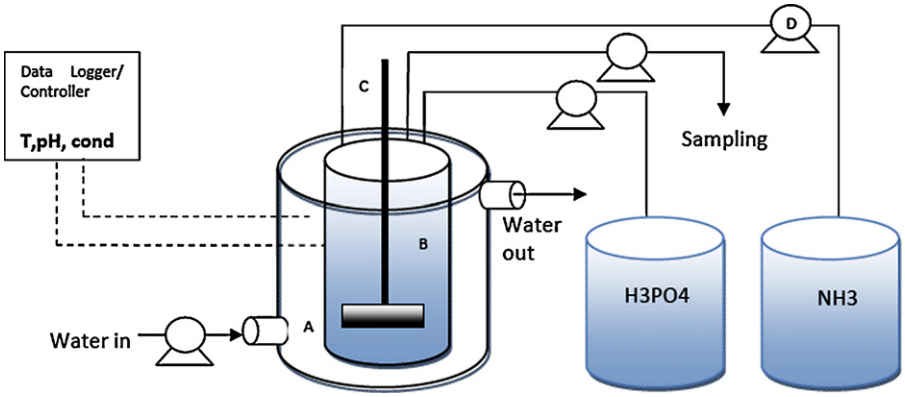

Fig. 1. Experimental setup: (A) cooling jacket; (B) vessel; (C) impeller and shaft; (D) peristaltic pump (all).

Table 2
Summary of experimental results for single feed systems (N/P: mole ratio of ammonia and phosporic acid, MV: mean size based on volume, MN: mean size based on numbers, and SD: standard deviation of MV).

Set	N/P	Δc [g/g sol]	MV [μm]	MN [μm]	SD [μm]	Yield [g/g sol]
45	0.79	0.088	252.3	109.8	92.35	0.080
44	0.85	0.107	399.47	56.332	184.01	0.051
42	0.91	0.125	393.53	21.235	168.11	0.108
46	0.99	0.149	443.44	14.706	79.37	0.145
39	1.08	0.138	439.16	16.751	94.47	0.080
47	1.18	0.136	396.79	15.184	112.06	0.070
38	1.28	0.112	362.72	22.863	0.03	0.148

N/P ratio has finer crystals, as the amount of solids formed is small and they do not have time to grow. A high ratio (1.28) gives coarser crystal size. From Ref. [16], it is known that MAP is least soluble at an N/P ratio of about 1.0 and most soluble at 1.4. It is clear that the CSD results correlate well with the MAP solubility. An N/P closer to 1.0 is experimentally proved and could result in the lowest solubility of salt and produce MAP crystal. DAP crystal cannot be formed in the system of 40 wt% phosphoric acid solution and 28 wt% ammonia solution due to its high solubility. TAP, on the other hand, can easily be produced when the pH reaches more than 8.0.

3.2. Non-seeded reactive crystallisation

As a comparison, a study of non-seeded reactive crystallisation was performed by varying the amount of MAP saturated solution used and feeding with the same amount of reactants at N/P molar ratio equal to 1. A CSD analysis for the final product was performed and is shown in Fig. 3. When only a small amount of MAP saturated solution was used, a higher supersaturation condition was reached due to a smaller amount of solvent. Consequently, higher supersaturation is generated and smaller crystal size produced. The mean size of the crystals increases steadily from 300 μm to 450 μm as the capacity of the crystalliser increases from 100 g to 300 g of MAP saturated solution. The CSD in number result corroborates the volume density results, but at the 300 g figure, the profile is lower than at 200 g. It is believed that this can happen due to the needle shape, which leads to a high breakage possibility in the suspension, or in the sampling and solid form. The shape of high supersaturation is tetragonal, which is close to a round shape. Therefore, the shape factor of a sphere can be used to predict the CSD in number while the needle crystals by having the shape factor deviated from the sphere's shape factor, might lead to a degree of error in these predictions. The non-seeded crystal at low supersaturation has a larger aspect ratio (H/W) compared to seeded crystallisation, which will be discussed in the next section.

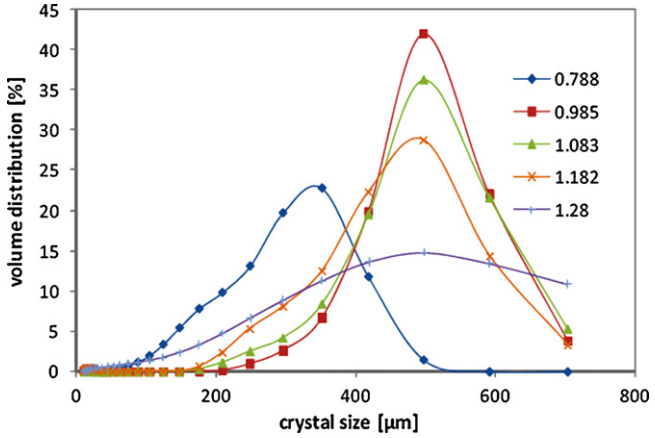

Fig. 2. CSD (as mass) of single feed system with 40 wt% for various N/P.

When a dual feed system was used, the phosphoric acid and ammonia solution at molar ratio (N/P) were equal to 1.0 and was titrated from a fixed point below the surface of saturated/supersaturated mono-ammonium phosphate. The total combined flow rate of the dual feed system at a high flow rate and a low flow rate was 4.45 g/min and 1.96 g/min respectively. Total default feeding time when a high flow rate was used was 5 min and 11 min when a low flow rate was applied. Total batch time ranged from 45 min to 90 min, but a 60 min batch time was generally employed.

Non-seeded reactive crystallisation experiments were conducted, since the primary and secondary nucleation takes place prior to crystal growth, and a significantly different behaviour can be observed when employing seed crystals. The supersaturation profile increases initially as feeding starts and the reaction takes place. During the feeding time, the nucleation process takes place; however, the supersaturation does not decline. The reason for this is that the reaction rate is much higher than the nucleation rate; therefore, the MAP solute was accumulated in the solution. Another explanation is that there is a higher dynamic solubility

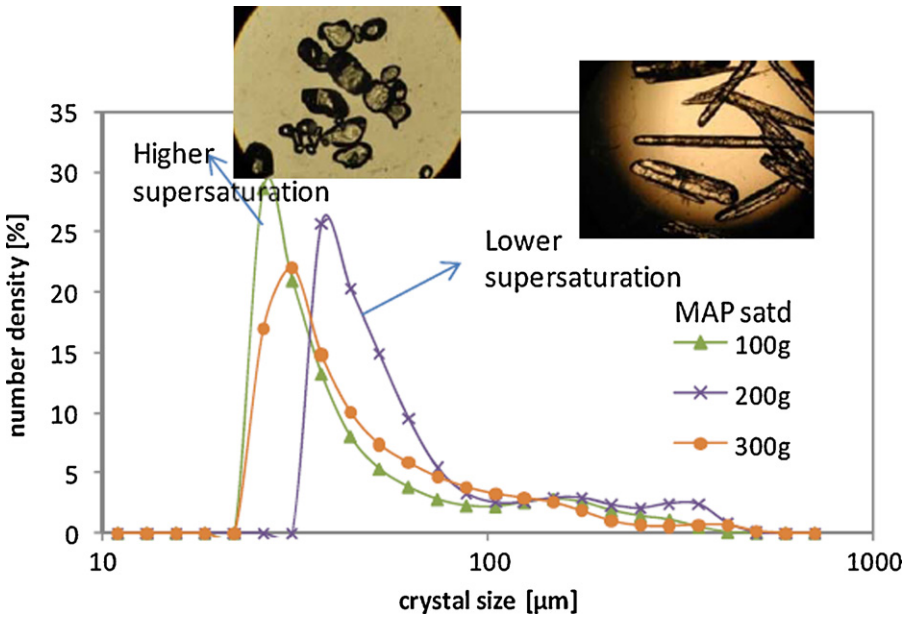

Fig. 3. CSD (as number) in non-seeded system for various initial capacities of MAP saturated. (inset: photo of crystals in the 100 g (left) and 300 g MAP saturated).

as the temperature increases slightly. If compared with the supersaturation profile for the non-seeded and non-reactive (NS/NRx) from Fig. 4, it is shown that the induction time for the non-reactive system is much longer than the reactive, as the maximum supersaturation is almost doubled. The nucleation rate is inversely related to induction time, and therefore, a higher nucleation rate for non-seeded reactive to a non-seed, non-reactive system can be predicted. It can be seen that in the non-seeded system, the primary and secondary nucleation is the rate controlling step. A general conclusion can be drawn from the CSD profiles, the non-seeded reactive crystallisation has a wider size distribution due to domination of nucleation and growth processes which happen subsequently from the initial stage.

In order to validate the fact that a reaction occurred between ammonia and phosphoric acids, an X-ray diffraction analysis of two powder samples was conducted. One sample was taken from the dual feed experiment, non-seeded (Set-93) which had a supersaturated MAP solution initially. Another tested sample was taken from a single feed experiment, N/P = 0.79, which had a phosphoric acid solution initially (Set-45). The Set-45 result indicates that the MAP is a major product component and some traceable impurities from the source of phosphoric acid may be detected as well. A more clear result can be seen from the Set-93 result which has higher intensity as a basis result. Further validation with the standard pattern of X-ray diffraction from JCPDS no. 37-1479 [18] shows a perfect agreement in both cases. This concludes that the MAP was produced both in single and dual feed systems.

3.3. Seeded reactive crystallisation

The seeded crystallisation behaves differently to the non-seeded one. In typical seeded crystallisation, the supersaturation level directly decreases during the process; crystal growth is controlled at all time while, in addition, a secondary nucleation may take place in the form of contact nucleation. Under the same operating conditions, the dynamic supersaturation of the non-reactive seeded system decreases more rapidly compared to the reactive seeded system. As in the reactive system, the solute mass balance is positive in the initial stage and becomes negative when the reaction is stopped.

Since a seeding policy reduces the nucleation process [19,20], growth will mainly take place in the seed crystals. Seed crystals grow in size while still maintaining the same width of size distribution as in the seed specification. Fig. 5 shows the non-seeded results in finer crystal and wider distribution compared to the 750 µm mean size and narrow distribution obtained from the seeded system. A small fraction of large crystals (1000–1500 µm) is produced

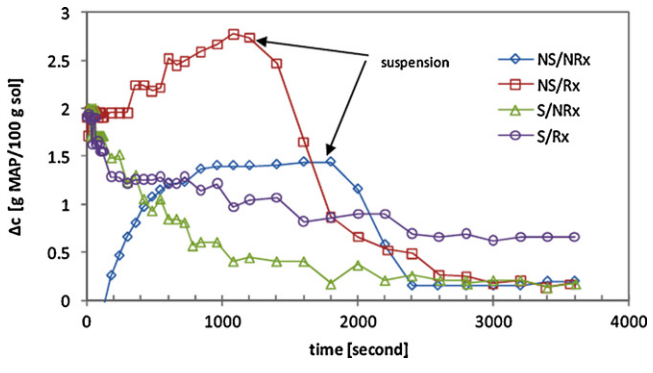

Fig. 4. Supersaturation profiles for various systems, NS: non-seeded, S: seeded, Rx: reactive, NRx: non-reactive.

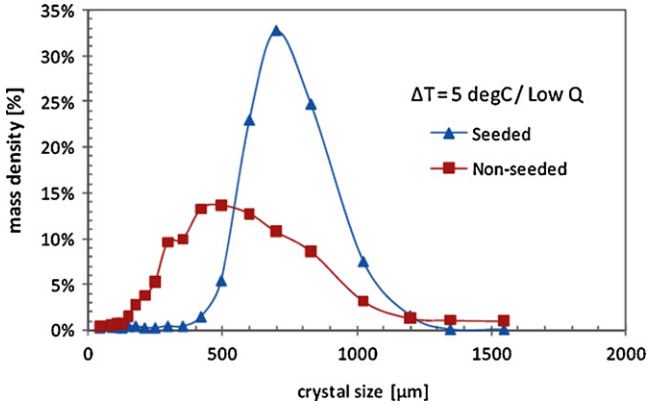

Fig. 5. CSD (as mass) for $\Delta T = 5\,^{\circ}C$, low flow rate both in seeded and non-seeded.

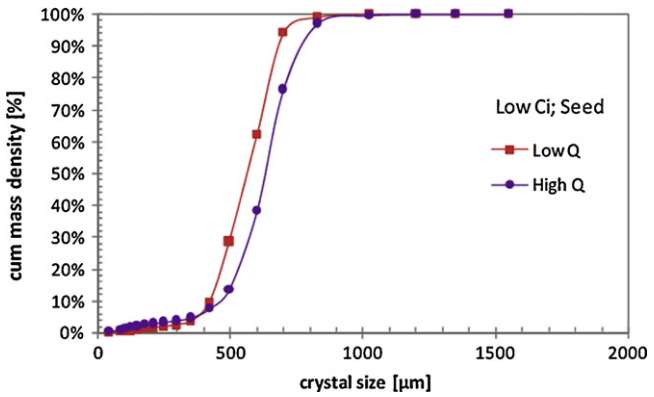

Fig. 6. Cumulative CSD (as mass) for seeded, low initial concentration, both in high/low flow rates.

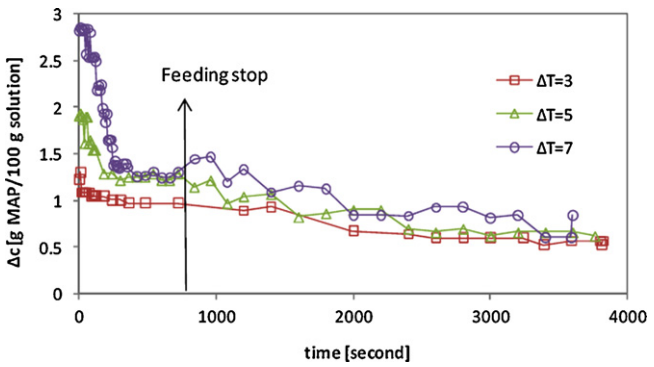

Fig. 7. Supersaturation profiles for various initial supersaturations, $\Delta T = 3\,^{\circ}C$, $5\,^{\circ}C$, and $7\,^{\circ}C$.

in the non-seeded system, which indicates primary nucleation takes place from the initial stage and a long period of growth process is taken by those crystals. While, subsequently, the secondary nucleation continues and only a short growth period occurs for the majority of the crystals. This is shown by the wide distribution of crystals lying from 40 μm to 800 μm.

3.4. Effect of feed flow rate

It is assumed that the feeding rate for both the ammonia solution and phosphoric acid causes altered CSD due to a different reaction rate and followed by different supersaturation profiles. A high flow rate triggers a maximum reaction rate due to higher reactant concentration in the system. An increase in temperature profile was observed in the high flow rate experiments, corroborating the fact that the reaction rate does increase and creates, therefore, higher local supersaturation and dynamic overall supersaturation levels at the initial stage. By maintaining a molar ratio (N/P) equivalent to 1, 4.45 g/min, total combined flow rate needs 5 min to reach 0.1–0.12 S/m increase in conductivity. The low flow rate experiment of 1.96 g/min requires 11 min to reach the same state. Some technical challenges faced during the experimental setup inhibited the choice below the minimum flow rate or higher than the maximum flow rate. This was due to the pump capacity and the vessel volume used. However, these challenges did not impede the study and some significant results were obtained and are presented in Fig. 6.

The high flow rate experiment results show a higher suspension density product. In the seeded system, the suspension density range is 4.0–4.5 g/100 g solution for the high flow rate and 3.5–4.0 g/100 g solution for the low flow rate. The higher flow rate, on the other hand, also causes finer crystals. This is due to the existence of a higher supersaturation level, which leads to more nucleation.

3.5. Effect of initial supersaturation

The supersaturation level is measured on-line by the conductivity method. In the seeded system, supersaturation is mainly used for seed growth. Secondary nucleation may occur at the same time, by initial breeding, fluid shear phenomenon, or a contact mechanism between crystals, crystalliser's wall – crystals and impeller – crystals. Fig. 7 illustrates desupersaturation profiles from three experiments that have different initial supersaturation. As expected, higher supersaturation generates a higher mass deposition rate and, therefore, sharper falls were observed. The high supersaturation ($\Delta T = 5$–$7\,^{\circ}C$) profiles consist of two parts of gradient: a high slope in the initial process and then a much lower gradient that occurs until the end of the batch. On the other hand, only one kind of gradient is observed in the low supersaturation experiment ($\Delta T = 3\,^{\circ}C$). At high supersaturation and with the presence of seed crystals, nucleation dominates the process in the initial stage causing a sharp drop in supersaturation profiles. The subsequent growth process can be described by the second slope (lower gradient), which is similar to the others.

The suspension density ranges from 1% up to 5% g solid per g solution. Secondary nucleation may occur due to hydrodynamic conditions and the physical state of the suspension. In the high suspension density that may have a significant fraction of coarse particles, secondary nucleation is easily triggered even though it is operating at a moderate state of mixing (300 rpm stirring speed was employed). Contact nucleation and breakage may occur at highest supersaturation ($\Delta T = 7\,^{\circ}C$). The total crystal number also increases greatly from 33,000 particles in the seed to 600,000–700,000 particles when $\Delta T = 5\,^{\circ}C$ and $\Delta T = 7\,^{\circ}C$ were used respectively (Fig. 8).

In addition to CSD, the shape of the crystal becomes an important feature for several applications. The knowledge of the crystal shape also helps the correct prediction of CSD measurement and in modelling. The aspect ratio of height (H) and width (W) of a crystal that was defined enabled the study to have more detail on the appropriate effects of supersaturation. Typically, a higher supersaturation leads to a higher aspect ratio. In this study, the lowest supersaturation ($\Delta T = 3\,^{\circ}C$) lead to an aspect ratio (H/W) of about 3.0–3.2, while the highest supersaturation ($\Delta T = 7\,^{\circ}C$) can produce an aspect ratio of about 1.5–1.9, as illustrated in Fig. 9.

3.6. Effect of feeding time

Feeding time is one of the key points in this study. Feeding allows the system to receive an additional mass of reactant to react, and to generate the supersaturation by producing more solute into the system. Total batch time in the semi-batch reactive crystallisation

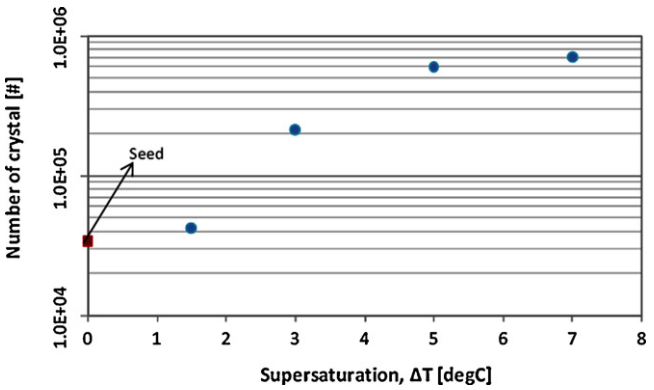

Fig. 8. The number of crystals of seeded system for various supersaturations.

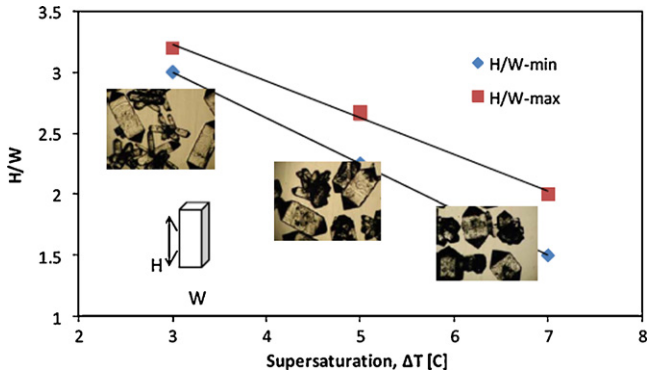

Fig. 9. Aspect ratio and crystal's images for several initial supersaturations.

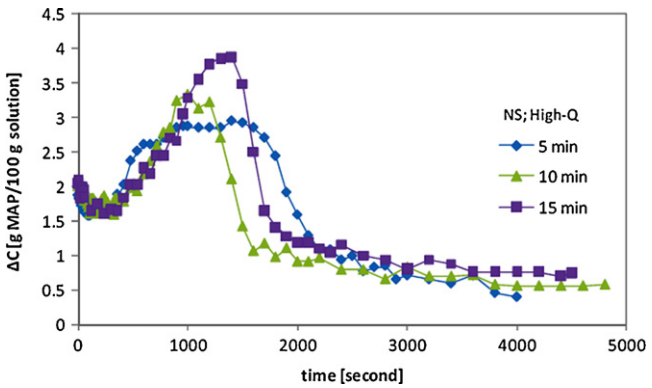

Fig. 11. Supersaturation profiles of non-seeded system for high flow rate and in several feeding times.

process consists of a feeding step in which the reaction takes place and a cooling step, where crystallisation and cooling occur. The basis of feeding time for the high flow rate is equal to 5 min, and 11 min for the low flow rate operation. Both feeding time conditions are theoretically and experimentally valid as they can produce the same amount of supersaturation. By observing the conductivity profiles of the non-seeded system, both conditions result in an 0.1–0.12 S/m increase in conductivity.

Three distinct CSD profiles in Fig. 10 show that the feeding time affects different crystal size distributions in the seeded system. A longer feeding time denotes more MAP solute produced in the system. This causes higher supersaturation and higher crystal yield. The supersaturation profile for 5 min drops quickly because only a small quantity of solute is produced in a short time period and the seed crystals continue to grow by consuming the remaining supersaturation. In the case of 22 min, there is a net production of solute due to limiting the seed crystals' ability to "eat" the supersaturation. Finally, a very high supersaturation resulted, which triggers more nucleation and growth of new nuclei. The supersaturation profile does fall during the end of batch time and finer crystals are produced.

For a non-seeded operation, as shown in Fig. 11, supersaturation profiles form a bell-curve followed by a slight decreased figure. A longer feeding time shapes a higher overshoot of supersaturation. The shorter time gives a longer induction period prior to spontaneous nucleation and, finally, a suspension state is reached. As expected, a higher total number of nuclei and smaller nuclei were produced in 10 min and 15 min feeding compared to the basis time. The falling area (L-shape) in the supersaturation figure consists of two parts. The first quick drop illustrates both the nucleation and growth process, and the second drop demonstrates crystal growth only. The first drop profile has a higher rate due to the high surface area of generated nuclei, followed by rapid growth.

3.7. Effect of mixing

Fluid mixing is an important factor in this study. Since perfect-mixing conditions are assumed, efforts have been made in the experimental setup to ensure a constant well-mixed regime in every run. Vessel geometry and shape, impeller size, and placement were coupled with the liquid hold up, and stirring speed caused a certain flow pattern in the crystalliser. It could be said that macro-scale mixing, which involves the overall flow pattern in the crystalliser, affects particles with a size of 1000 μm or larger. The ratio of power input and fluid capacity will only govern the particles that are the size of 100 μm or smaller in a micro-scale environment. In this study, the geometry and the liquid hold up is kept constant while a decrease in the stirring speed was employed to check the imperfect mixing conditions, both in the high and low flow rate operations in the seeded reactive crystalliser.

In high flow rate conditions, the rapid production of solute can only be utilised by a smaller amount of crystal because, at a low stirring speed, the remaining crystals stay un-mixed in the bottom of the crystalliser. The surface area of active crystals is significantly reduced, therefore the same amount of supersaturation will only benefit and grow active crystals larger than the conditions of a well-mixed system at 300 rpm. On the other hand, in the low flow rate operation, the solute generation is moderate and, even in 200 rpm mixing, the growth rate of active crystals can compete, because a low supersaturation level was maintained. By observing the supersaturation history in Fig. 12, it can be seen that when using the high flow rate and the low stirring speed, the profile deviates in the initial

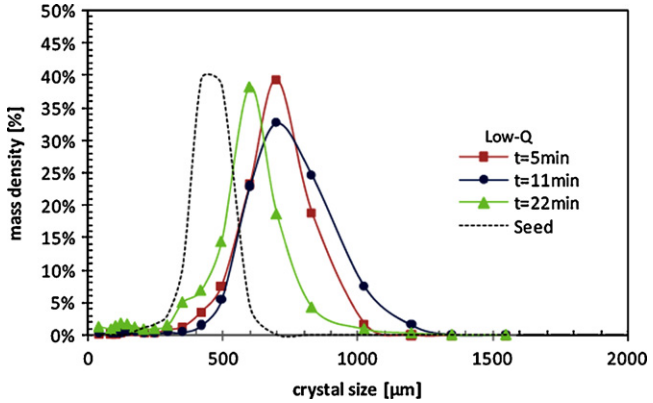

Fig. 10. CSD (as mass) for seeded system for low flow rate and in several feeding times.

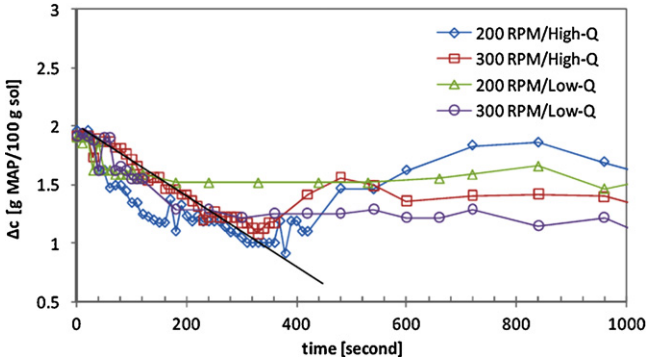

Fig. 12. Supersaturation profiles of seeded systems for high/low flow rate at 200 rpm and 300 rpm.

stage due to different degrees of reaction. Once the crystals are large enough, they stay in the bottom and the total active surface area is progressively reduced. It can be concluded that the seeded reactive system under study behaves differently and the micro-mixing is an important factor to consider in a small scale experiment. For a non-seeded reactive system, as mentioned in published works [13,14], a decrease in stirring speed may cause a decrease in nucleation rate and/or an increase in growth. As a result, a higher suspension density and mean size are expected. However, most of the previous works which discussed the mixing in a reactive system have been done only for a low solubility product.

4. Concluding remarks

In conclusion, both single feed and dual feed systems can produce mono-ammonium phosphate crystals. These have been verified by X-ray diffraction analysis and validated with the standard XRD pattern of MAP. For a single feed system, a reactant's N/P molar ratio controls the degree of reaction and thus governs the crystal size distribution of the product. An N/P closer to 1.0 is experimentally proved that results in the lowest solubility and produce MAP crystals. DAP crystals cannot be formed in the system due to its high solubility. TAP, on the other hand, can easily be produced when the pH reaches more than 8.0. The CSD of single feed system is smaller and wider than the dual feed system. This indicates that nucleation is more dominant in a single feed system.

In a non-seeded system, the nucleation process prevails. The supersaturation profiles increase and stay constant for some period of induction time before a visible nuclei starts. The induction time is significantly long, which constitutes almost one-third (1/3) of the total batch time. A seeding policy is essentially needed to minimise the impact of the nucleation process. Therefore, a wider crystal size distribution can be avoided. The higher flow rate causes finer crystals. This is because of the existence of a higher supersaturation level, which leads to more nucleation. The reaction kinetics is affected, as the higher concentrations of reactants exist when higher flow rates were applied. On the other hand, due to the fast reaction, at a low flow rate, the accumulation of reactant's concentration is negligible during the feeding time. The temperature rises due to higher reaction rates altering the solubility dynamic and affecting the final product size distribution.

In a seeded system, supersaturation is mainly used for seed growth. At high supersaturation and the presence of seed crystals, nucleation dominates the process in the initial stage and can cause a sharp drop in supersaturation profiles. The subsequent growth process can be described by the second moderate slope, which is similar to others. On the other hand, at low supersaturation, only growth is dominant for the whole process. In this study, lower supersaturation also leads to a needle shape, which is undesirable and altered from the normal structure of MAP crystal, which has a cubical or tetragonal bipyramid shape.

Feeding time is one of the important factors in this study. In a seeded system, the longer feeding time denotes more MAP solute produced in the system. This causes higher supersaturation and higher crystal yields. For a non-seeded operation, supersaturation profiles form a bell-curve followed by a slight decreased figure. A longer feeding time shapes a higher overshoot of supersaturation. The shorter time gives a longer induction period prior to spontaneous nucleation and, finally, a suspension state was reached. For mixing intensity factors, it can be concluded that the seeded reactive system under study behaves differently and the meso- and micro-mixing is an important factor to consider in a small-scale experiment because the reaction occurs on a molecular scale.

Acknowledgements

The first author acknowledges the support from Curtin International Research Tuition Scholarship (CIRTS) for his studies, Hyogo University Mobility in Asia and Pacific (HUMAP) scholarship during his research work in University of Hyogo, Japan, and the Learning Support Network at Curtin University of Technology for providing a proof-reading support.

References

[1] W.H. Ross, A.R. Merz, K.D. Jacob, Preparation and properties of the ammonium phosphates, Ind. Eng. Chem. 21 (1929) 286–289.
[2] B. Bernard-Michel, M.N. Pons, H. Vivier, S. Rohani, The study of calcium oxalate precipitation using image analysis, Chem. Eng. J. 75 (1999) 93–103.
[3] B.L.A. Slund, A.K.C. Rasmuson, Semibatch reaction crystallization of benzoic acid, AIChE J. 38 (1992) 328–342.
[4] M. Ståhl, B.L.A. Slund, A.C. Rasmuson, Reaction crystallization kinetics of benzoic acid, AIChE J. 47 (2001) 1544–1560.
[5] O. Söhnel, J.W. Mullin, Precipitation of calcium carbonate, J. Cryst. Growth 60 (1982) 239–250.
[6] W.N. Al Nasser, A. Shaikh, C. Morriss, M.J. Hounslow, A.D. Salman, Determining kinetics of calcium carbonate precipitation by inline technique, Chem. Eng. Sci. 63 (2008) 1381–1389.
[7] E. Uehara-Nagamine, P.M. Armenante, Semibatch precipitation of barium sulphate, Trans. IChemE 79 (2001) 979–988.
[8] M. Aoun, E. Plasari, R. David, J. Villermaux, A simultaneous determination of nucleation and growth rates from batch spontaneous precipitation, Chem. Eng. Sci. 54 (1999) 1161–1180.
[9] P.C. Chen, G.Y. Cheng, M.H. Kou, P.Y. Shia, P.O. Chung, Nucleation and morphology of barium carbonate crystals in a semi-batch crystallizer, J. Cryst. Growth 226 (2001) 458–472.
[10] F. Salvatori, H. Muhr, E. Plasari, J.M. Bossoutrot, Determination of nucleation and crystal growth kinetics of barium carbonate, Powder Technol. 128 (2002) 114–123.
[11] P.A. Barata, M.L. Serrano, Salting-out precipitation of potassium dihydrogen phosphate (KDP). I. Precipitation mechanism, J. Cryst. Growth 160 (1996) 361–369.
[12] Y. Kotaki, H. Tsuge, Reactive crystallization of calcium carbonate in a batch crystallizer, J. Cryst. Growth 99 (1990) 1092–1097.
[13] N.S. Tavare, J. Garside, Simulation of reactive precipitation in a semi-batch crystallizer, Chem. Eng. Res. Des. 68 (1990) 115–122.
[14] E. Abbasi, A. Alamdari, Mixing effects on particle size distribution in semi-batch reactive crystallization of maneb, J. Chem. Eng. Jpn. 40 (2007) 636.
[15] B. Zhong, J. Li, Y.X. Zhang, B. Liang, Principle and technology of ammonium phosphate production from middle-quality phosphate ore by a slurry concentration process, Ind. Eng. Chem. Res. 38 (1999) 4504–4506.
[16] G.R. Campbell, Y.K. Leong, C.C. Berndt, J.L. Liow, Ammonium phosphate slurry rheology and particle properties—the influence of Fe(III) and Al(III) impurities, solid concentration and degree of neutralization, Chem. Eng. Sci. 61 (2006) 5856–5866.
[17] J.L. Torgesen, A.T. Horton, Electrolytic conductance of ammonium dihydrogen phosphate solutions in the supersaturated solutions in the saturation region, Chem. Eng. Res. Des. 64 (1963) 109–118.
[18] D. Xu, D. Xue, Chemical bond analysis of the crystal growth of KDP and ADP, J. Cryst. Growth 286 (2006) 108–113.
[19] N. Doki, N. Kubota, A. Sato, M. Yokota, O. Hamada, F. Masumi, Scaleup experiments on seeded batch cooling crystallization of potassium alum, AIChE J. 45 (1999) 2527–2533.
[20] N. Kubota, N. Doki, M. Yokota, D. Jagadesh, Seeding effect on product crystal size in batch crystallization, J. Chem. Eng. Jpn. 35 (2002) 1063–1071.